ELSEVIER

Journal of Nuclear Materials 299 (2001) 53–67

journal of nuclear materials

www.elsevier.com/locate/jnucmat

Modeling of microstructure evolution in austenitic stainless steels irradiated under light water reactor condition

J. Gan [a,*], G.S. Was [b], R.E. Stoller [c]

[a] *Material Interface and Characterization Group, Pacific Northwest National Laboratory, MSIN P8-16, P.O. Box 999, Richland, WA, USA*

[b] *Nuclear Engineering and Radiological Sciences and Materials Science and Engineering, The University of Michigan, Ann Arbor, MI, USA*

[c] *Metal and Ceramic Division, Oak Ridge National Laboratory, TN, USA*

Received 28 November 2000; accepted 25 July 2001

Abstract

A model for microstructure development in austenitic alloys under light water reactor irradiation conditions is described. The model is derived from the model developed by Stoller and Odette to describe microstructural evolution under fast neutron or fusion reactor irradiation conditions. The model is benchmarked against microstructure measurements in 304 and 316 SS irradiated in a boiling water reactor core using one material-dependent and three irradiation-based parameters. The model is also adapted for proton irradiation at higher dose rate and higher temperature and is calibrated against microstructure measurements for proton irradiation. The model calculations show that for both neutron and proton irradiations, in-cascade interstitial clustering is the driving mechanism for loop nucleation. The loss of interstitial clusters to sinks by interstitial cluster diffusion was found to be an important factor in determining the loop density. The model also explains how proton irradiation can produce an irradiated dislocation microstructure similar to that in neutron irradiation. © 2001 Published by Elsevier Science B.V.

1. Introduction

Microstructure modeling is an important tool used to understand and predict microstructure development of metals and alloys under irradiation. The irradiated microstructure is believed to impact and even control critical processes such as void swelling, creep, stress relaxation, loss of ductility and fracture toughness. The development of the irradiated microstructure is governed by the complex interactions of numerous inter-dependent processes that depend on material and irradiation parameters. Understanding the impact and interdependence of these parameters becomes a daunting experimental task. However, if we are able to model the fundamental processes, we will be in a better position to understand and predict the development of the microstructure under irradiation and subsequent behavior of the irradiated material. An understanding of irradiated microstructure may also contribute to our understanding of current problems such as irradiation assisted stress corrosion cracking (IASCC) in LWR core materials.

Considerable effort was devoted in the 1970s and 1980s to develop an understanding of the void swelling observed in many structural materials when they are exposed to fast neutron irradiation. The initial work focused on the development of the basic concepts and point defect sink strengths required [1–4]. Later, detailed microstructure models were developed to describe the evolution of voids in stainless steels as part of national fast reactor and fusion materials programs [5–15], with other components of the irradiated microstructure (e.g., faulted loops, dislocation network etc.) receiving less attention. The work of Mayer et al. [12] on microstructure modeling was probably the most comprehensive among the early theoretical studies of microstructure evolution under irradiation. They developed a model to treat voids and clusters of

* Corresponding author. Tel.: +1-509 376 6372; fax: +1-509 376 6308.

E-mail address: Jian.Gan@pnl.gov (J. Gan).

0022-3115/01/$ - see front matter © 2001 Published by Elsevier Science B.V.
PII: S0022-3115(01)00673-0

Nomenclature

C_i, C_v	atomic concentration of point defects
C_2, C_3, C_4	atomic concentration of di-, tri- and tetra-interstitial
G_{dpa}	displacement rate
G_v	production rate of vacancies
η	cascade efficiency
f_2, f_3, f_4	fraction of interstitials surviving the cascade and in the form of di-, tri- and tetra-interstitials, respectively
f_{vcl}	fraction of in-cascade vacancy clusters
r_{vcl}	the radius of vacancy clusters
a_0	lattice constant
β_v^j, β_i^j $(j = 1–4)$	rate constant for the impingement of point defects on interstitial clusters of size j
β_j^v, β_j^i $(j = 2, 3, 4)$	rate constant for the reactions of an interstitial cluster of size j with an interstitial or a vacancy
β_j^k $(j = 2, 3$ & $k = 2, 3, 4)$	rate constant for the reaction between interstitial clusters
z_i^j, z_v^j $(j = 1–4)$	interstitial or vacancy combinatorial number for interstitial clusters
E_2^i, E_3^i	rate constant for the thermal dissociation of di- and tri-interstitials
D_v, D_i, D_{ij} $(j = 2, 3, 4)$	diffusivity of vacancy, interstitial and interstitial clusters
α	point defect recombination coefficient
S_i^j, S_v^j	extended defect sink strengths where: $j =$ 'n' for network dislocations, 'L' for faulted loops, 'cvt' for cavities (bubble and/or voids), 'vcl' for vacancy clusters and 'g' for subgrain structure
S_i^T, S_v^T	sum of the extended sink strength
τ_4	the lifetime of the tetra-interstitial before it grows into the 1st size class of loops

vacancies and interstitials, as well as dislocation loops. However, the major focus of their model was void swelling and little attention was given to dislocation microstructure.

Stoller and Odette [16,17] developed a more comprehensive model of microstructure evolution in austenitic stainless steel under fast neutron irradiation conditions. Their model focused on the interactions between point defects and the evolving dislocation and cavity microstructures to understand the temperature and neutron fluence dependence of void swelling. Void swelling levels, the total dislocation density, and faulted interstitial loop density were generally well predicted by the model. The primary shortcomings of their model were a relatively poor description of the dislocation loop size distribution and an under prediction of the loop density at temperatures below about 400 °C.

A similarly detailed model of microstructure evolution in austenitic stainless under LWR irradiation conditions has not been reported in the literature. In addition, the experimental database from post-irradiation microstructural examination of relevant materials has been insufficient to aid in the development and verification of such a model. The database from fast reactor and fusion program experiments is of limited value since LWR core internal components operate at much lower temperatures than was typically examined (~300 °C vs 400–650 °C) in these experiments. The lower temperature will lead to higher nucleation rates for defects such as dislocation loops, implying that an improved model with a more detailed treatment of dislocation loop microstructure will be required to fully describe microstructural evolution under these irradiation conditions.

Proton irradiation is becoming an extremely useful tool for emulating neutron irradiation. Under the proper irradiation conditions, proton irradiation can produce a microstructure and microchemistry very similar to that of neutron irradiation [18–20]. The similarity of the irradiated microstructure between neutron and proton irradiation was initially surprising given the known difference in cascade morphology, damage efficiency and damage rate. Clearly, the processes governing the formation and growth of the dislocation microstructure must be quite similar or there are compensating effects. By modeling and benchmarking the proton-irradiated microstructure against that from neutrons using the same model, we can gain insight into the similarities and differences in processes governing the microstructure evolution. Given the tremendous advantage of proton irradiation over neutron irradiation in time, cost and sample activation, the motivation for developing the capability to predict the proton-irradiated microstructure is high.

In this paper, we first present a brief description of the Stoller and Odette microstructure (SOM) model for microstructure evolution under fast reactor conditions. The model is then modified and adapted for irradiation conditions in light water reactor cores. Parameter selection and determination is made using measurements of dislocation loop density and size as function of dose. Once the model for LWR neutron irradiation is established and benchmarked, modeling of proton irradiation

relevant to LWR neutron irradiation will be treated. The major issues such as in-cascade interstitial clustering, damage efficiency and the loss of small interstitial clusters to the sinks by cluster diffusion are addressed and incorporated into a version of the model that is relevant to proton irradiation. Finally, insights into physical processes governing the dislocation loop microstructure are summarized.

2. The SOM microstructure model for fast reactors irradiation conditions

The SOM model is described in detail in [16,17]. This model is based on the reaction rate theory, and was developed to investigate void swelling and microstructural evolution under fast reactor and fusion reactor irradiation conditions. It applies to the temperature range 350–700 °C for doses up to 100 dpa. It calculates the dose dependence of void swelling, the faulted loop density and average loop size, network dislocation density and total dislocation density. The nucleation, growth and unfaulting of Frank loops are treated in the model. The growth of cavities and the conversion of bubbles to voids, as well as void swelling, are included, but cavity nucleation is not treated in the SOM model. It also describes the dose dependence of the concentrations of vacancies, interstitials, di-, tri- and tetra-interstitials as well as vacancy clusters. The major uncertainties in the SOM model are in the material parameters (for example, point defect biases and diffusivities) which are not altered to reflect either spatial or temporal fluctuations in the alloy composition.

The first step required to apply the SOM model to LWR irradiation is the adjustment of irradiation parameters. The difference in irradiation parameters between a fast reactor and a LWR is shown in Table 1. However, when the model was applied to irradiation conditions relevant to LWR cores (lower temperature, lower dose) by simply adjusting the irradiation parameters, it severely underestimated the loop density. This is consistent with the earlier observation that faulted loop densities tended to be too low below about 400 °C [16]. Using the LWR irradiation parameters in the SOM model, the dose dependence of the dislocation loop density for the LWR case is shown in Fig. 1, along with the experimental data [22]. The calculated loop density is about two orders of magnitude lower than the experimental data. The calculated loop diameter is in better agreement with the measurement. Since the model assumes only classical or stochastic nucleation of faulted loops through point defect diffusion and clustering, the severe underestimate of loop density indicates that classical nucleation alone is not enough to account for the measured loop densities. The difference between the predicted and observed loop density suggests that a direct application of the SOM model to the LWR condition is not appropriate, especially since the major microstructure feature in LWRs is the faulted loop rather than the void.

Table 1
Irradiation parameters used for fast reactor and LWR irradiation conditions

	Fast reactor	LWR core
Dose rate (dpa/s)	1×10^{-6}	$(2–11) \times 10^{-8}$[a]
Dose (dpa)	Up to 100	<20
Temperature (°C)	400–700 [21]	270–340
Helium (appm/dpa)	0.35	2.3[b]

[a] Data are extracted from irradiations in a commercial BWR (Barseback 1 BWR, ABB).
[b] Value is estimated from the work done by F. Garner at PNNL.

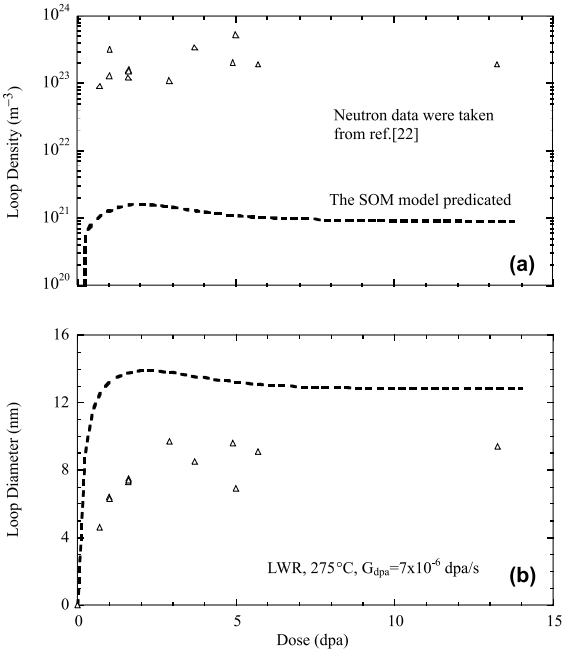

Fig. 1. Dose dependence of faulted loop density (a) and size (b) for austenitic stainless steel irradiated in LWR at 275 °C, calculated from the SOM model. In-cascade interstitial clustering and diffusion of interstitial clusters are not included. Neutron data were taken from [22].

3. Modeling of microstructure evolution under LWR irradiation conditions

3.1. Rationale for modifications to the SOM interstitial clustering model

A mechanism for nucleating loops directly from in-cascade interstitial clustering was introduced onto the

SOM model. This decision is consistent with results from recent MD simulations of primary damage formation [23,24] and our empirical observation that classical nucleation is not adequate to account for the observed loop nucleation under LWR conditions. The MD simulations indicate that a significant fraction of the interstitials produced in displacement cascades form small clusters during the cascade event. The cascade-produced clusters would greatly increase the loop nucleation rate by providing stable nuclei directly, without requiring any stochastic clustering reactions. The fraction of in-cascade interstitial clustering varies from less than 20% of the surviving interstitials at 200 eV (relevant to MeV proton irradiation) to ~50% at 10 keV (relevant to MeV neutron irradiation). The PKA spectrum-averaged interstitial clustering fraction is nearly constant for several different types of neutron irradiation environments. Other experimental evidence [25–28] also supports in-cascade interstitial clustering as the dominant loop nucleation mechanism in LWR irradiation conditions. Yoshida et al. [25,28] found that the saturated density of interstitial loops in pure Fe–Cr–Ni alloy estimated from classical nucleation was about 3 orders of magnitudes lower than that measured for neutron irradiation at 290 °C ($\sim 10^{23}$ m^{-3}).

In addition to supporting the important role of in-cascade formation of interstitial clusters, both experimental evidence [29] and MD calculations [30–34] suggest that small interstitial clusters are very mobile and can therefore be lost to the sinks by diffusion. According to the work in [31,34], the formation energy for interstitial clusters increases with cluster size as expected, but the migration energy for interstitial clusters decreases as the cluster size increases. For example, MD results [34] for Cu show that the migration energy for a single self-interstitial-atom (SIA) is 0.082 eV, and that for di-, tri- and tetra-interstitials are 0.05, 0.013 and 0.005 eV, respectively. Other MD results [31] show a migration energy of 0.025 eV for di-interstitials in Cu. Similar results have been obtained for iron [24]. It is interesting to note that these very low migration energies are on the order of the kinetic energy of lattice atoms at room temperature ($\sim kT = 0.025$ eV at 300 K). This indicates that the clusters must migrate in an essentially athermal fashion.

With such low migration energies, the small clusters would rapidly diffuse to sinks and be lost from the system, particularly if the clusters exhibit preferential one-dimensional motion as observed in the MD simulations [23,24,35]. This would reduce their impact on loop nucleation. Although the MD simulations indicate that interstitial cluster motion is primarily one-dimensional in close-packed directions, the smallest clusters frequently change from one close-packed direction to another, giving a net migration behavior that is nearly equivalent to three-dimensional random walk [35,36]. Finally, it must be recognized that the MD results are for 'computer pure' materials described by an interatomic potential that is only an approximation of the material in question. Even if the interatomic potentials used are sufficiently accurate, they do not account for the effects of defect trapping by solutes or impurities which would reduce the cluster mobility in real metals and alloys.

In summary, the high levels of in-cascade clustering observed in the MD simulations should provide a significant loop nucleation mechanism that is not accounted for in the SOM model. However, simply applying the clustering fractions obtained from these simulations may well overstate the impact of the mechanism because the low cluster migration energies would lead to their being lost to sinks. Thus, in-cascade clustering is expected to contribute to interstitial loop nucleation, and the differences in the primary recoil spectra between neutron and proton irradiations will give rise to different clustering behavior between the two environments. Uncertainties about several details of the cluster migration behavior such as the relative importance of one-dimensional migration and the impact of solute trapping make it difficult to specify the relevant material parameters in the model. The MD results were used to provide guidance for initial parameter choices, but these parameters were then varied in the process of fitting the prediction of the revised SOM model to the experimental data.

3.2. Modifications to the rate equations

The two modifications made to the SOM model were to include in-cascade interstitial clustering as a source term in the rate equations, and to permit the small interstitial clusters to migrate. As a first approximation, it was assumed that only di-, tri- and tetra-interstitial clusters are produced by in-cascade interstitial clustering. This decision is partially guided by the MD results which indicate that fraction of interstitials in cluster sizes greater than about 4 is not large [23]. Similarly, only these smallest interstitial clusters were assumed to be mobile. In both cases, this approximation provides a way of exploring the physical mechanisms involved without adding undue complexity and parameters to the model. The impact of including larger in-cascade clusters needs to be explored. Based on the discussion presented above, the small interstitial clusters were assumed to migrate in three-dimensions rather than one-dimensionally. For simplicity, it was assumed that the extended defect sink strength for small interstitial clusters is the same as that for a single interstitial. All of these assumptions may not be strictly warranted, but they provide a reasonable approach for including relevant physical mechanisms in the model.

Compared to those in the SOM model, the rate equations for the modified model include several new terms. The new terms are highlighted by boxes in the modified rate equations which follow:

$$\frac{dC_v}{dt} = G_v - \beta_v^2 C_2 - \beta_v^3 C_3 - \beta_v^4 C_4 - \alpha C_i C_v - D_v C_v S_v^T \boxed{-\beta_2^v C_v - \beta_3^v C_v - \beta_4^v C_v}, \quad (1)$$

$$\frac{dC_i}{dt} = G_i + C_2(2E_2^i + \beta_v^2 - \beta_i^2) + C_3(E_3^i - \beta_i^3) - \beta_i^1 C_i - \beta_i^4 C_4 - \alpha C_i C_v - D_i C_i S_i^T \boxed{+\beta_2^v C_v - \beta_2^i C_i - \beta_3^i C_i - \beta_4^i C_i}, \quad (2)$$

$$\frac{dC_2}{dt} = \boxed{\eta G_{dpa} \tfrac{f_2}{2}} + \beta_i^1 \frac{C_i}{2} + C_3(\beta_v^3 + E_3^i) - C_2(\beta_v^2 + \beta_i^2 + E_2^i) \boxed{-D_{i2} C_2 S_i^T + \beta_3^v C_v - \beta_2^v C_v - \beta_2^i C_i} \boxed{-2\beta_2^2 C_2 - \beta_2^3 C_3 - \beta_2^4 C_4}, \quad (3)$$

$$\frac{dC_3}{dt} = \boxed{\eta G_{dpa} \tfrac{f_3}{3}} + \beta_i^2 C_2 + \beta_v^4 C_4 - C_3(\beta_v^3 + \beta_i^3 + E_3^i) \boxed{-D_{i3} C_3 S_i^T + \beta_2^i C_i + \beta_4^v C_v - \beta_3^v C_v - \beta_3^i C_i} \boxed{-\beta_3^2 C_2 - 2\beta_3^3 C_3 - \beta_3^4 C_4}, \quad (4)$$

$$\frac{dC_4}{dt} = \boxed{\eta G_{dpa} \tfrac{f_4}{4}} + \beta_i^3 C_3 - \beta_v^4 C_4 - C_4 \tau_4^{-1} \boxed{-D_{i4} C_4 S_i^T + \beta_3^i C_i - \beta_4^v C_v + \beta_2^2 \tfrac{C_2}{2}}, \quad (5)$$

where

$$G_i = \eta G_{dpa} \boxed{(1 - f_2 - f_3 - f_4)}, \quad (6)$$

$$S_v^T = S_v^n + S_v^L + S_v^{cvt} + S_v^{vcl} + S_v^g, \quad (7)$$

$$S_i^T = S_i^n + S_i^L + S_i^{cvt} + S_i^{vcl} + S_i^g. \quad (8)$$

In the modified rate equations, G_i is the single interstitial production rate, f_2, f_3 and f_4 are the fractions of interstitials surviving the cascade and in the form of di-, tri- and tetra-interstitials, respectively, S_v^T and S_i^T are the total extended sink strengths in Eqs. (1)–(5) [16]. The additional rate constants required to account for interstitial cluster mobility are: β_j^i and β_j^v for the reactions of an interstitial cluster of size j ($j = 2, 3, 4$) reacting with an interstitial or a vacancy, respectively (due to interstitial cluster diffusion), β_j^k for the reactions between interstitial clusters ($j, k = 2, 3, 4$):

$$\beta_j^i \approx \frac{z_i^j D_j C_j}{a_0^2}, \quad (9)$$

$$\beta_j^v \approx \frac{z_v^j D_j C_j}{a_0^2}, \quad (10)$$

$$\beta_j^k \approx \frac{z_i^k D_j C_j}{a_0^2}, \quad (11)$$

where a_0 is lattice constant, z_i^j, z_v^j are the interstitial or vacancy combinatorial numbers [16,37]. More details on the modifications to the SOM model can be found in [38].

3.3. Parameters for LWR neutron irradiation

The experimental data used to calibrate the modified SOM model were generated from a commercial BWR (Barseback 1, ABB). According to [39], the irradiation occurred at 275 °C at fluxes from 1.5×10^{13} to 7.6×10^{13} n/cm^2/s ($E > 1$ MeV). This corresponds to a dose rate of 2.2–11×10^{-8} dpa/s. A dose rate of 7×10^{-8} dpa/s was used as the reference value for the model calculations. Since the MD results indicate that the spectrum-averaged cascade efficiencies are nearly the same for different neutron irradiation environments, a cascade efficiency of 0.33 is used for LWR irradiation [40]. In addition to the irradiation parameters of temperature, dose-rate and cascade efficiency, the principal task is to determine the effective material and irradiation parameters used to describe defect behavior under LWR conditions. These are: fractions of in-cascade interstitial clustering for di-, tri- and tetra-interstitials, fraction and size of in-cascade vacancy clusters, and pre-exponential terms in the diffusivity for di-, tri- and tetra-interstitials.

Based on the MD results [23,40], it was assumed that the fraction of in-cascade interstitial clustering is about 42–50% of the surviving defects, with $f_2 = f_3 = 20\%$ and $f_4 = 2$–10%. Since the tetra-interstitial is treated as the stable nucleus for loops, the model calculation is expected to be more sensitive to f_4. The actual value of f_4 will be determined by the fit between model and data as discussed later. In-cascade vacancy clustering has also been investigated by MD simulations, but the results are somewhat more ambiguous than for the interstitials [24]. Initial values for the fraction of vacancies contained in such clusters (f_{vcl}) and the size of vacancy cluster (r_{vcl}) were taken from the SOM calibration for fast reactor irradiation. The final value for f_{vcl} was determined with comparisons between model calculations and the data.

Instead of using the migration energy generated from MD simulations, the migration energy for di-, tri and tetra-interstitials was treated the same as for a single interstitial. This follows the approach of the SOM model and is consistent with experimental measurements in Fe–Cr–Ni alloys, with the relatively high value arising from solute trapping [16]. For stainless steels, a migration energy of 0.85 eV has been used for a single interstitial [16] and for interstitial clusters. This value is based on the fit of the SOM model to fast reactor data, and is consistent with experimental measurements in Fe–Cr–Ni alloys [16,41,42]. The difference between this and the lower values obtained from experimental measurements in pure metals [43] and from the MD results is attributed to solute and impurity trapping. The MD results indicate that the pre-exponential term for cluster mobility decreases as the cluster size increases [35]. For a single

interstitial, the value of the pre-exponential term (D_i^0) was chosen from the original SOM model, 0.08 cm^2/s. The pre-exponential terms in the diffusivity for di- and tri-interstitials were takes as $D_2^0 = D_3^0 = 0.01$ cm^2/s, a factor of 8 lower than that of a single interstitial, and the value of D_4^0 was determined by the fit between the model and data as discussed later. The other approximations in the model include the following:

- Vacancy clusters are all of one size class.
- Vacancy clusters are treated as immobile.
- The cascade efficiency is assumed to be dose independent, although it could be treated as a function of dose since pre-existing defects may reduce the cascade survival once cascade overlaps occur.

3.4. Parameters for proton irradiation

Proton irradiation parameters are quite different from those used obtained under neutron irradiation due to the difference in energy transfer from particles to lattice atoms. In the calculation for proton irradiation, a damage rate of 7×10^{-6} dpa/s and an irradiation temperature 360 °C were used. These conditions were selected in order to create an irradiated microstructure that was similar to that generated in Barseback-1 reactor. For 3.2 MeV proton irradiation of iron, the average energy transferred to the lattice atoms through Coulomb interaction can be calculated using standard methods [44] as 228 eV. From the MD results presented in [40], the corresponding cascade efficiency (per NRT displacement) is 0.9, and the in-cascade interstitial clustering fraction (per surviving interstitial) is in the range 0–0.25 over the temperature range 100–900 K.

As discussed earlier, proton irradiation generates well-separated cascades of much smaller size than does neutron irradiation. Therefore a significant reduction of in-cascade interstitial clustering should be expected. Note that the average damage energy for iron irradiated by 1 MeV neutrons is about 20 keV, which is about 100 times higher than the 228 eV value for a 3.2 MeV proton. Based on the MD results in [40], the fraction of in-cascade interstitial clustering used for proton irradiation was assumed to be a factor of 10–20 lower than that for neutron irradiation. Therefore for proton irradiation, we initially set $f_2 = f_3 = 1$–2% and $f_4 \approx 0.1$–0.2%. The exact values were determined by fit to the proton data.

4. Results and discussion

Using the parameters discussed in the previous sections, a series of computations were made to determine the dose, dose-rate and temperature dependence of dislocation loop density and size according to the following logic:

1. Determine a set of parameters for LWR irradiation conditions (275 °C, 7×10^{-8} dpa/s) that provides a fit between model and data.
2. Use the LWR parameter set as a reference case and check the dose-rate dependence (at 275 °C) and the temperature dependence (7×10^{-8} dpa/s) of loop density and size as an intermediate condition in moving from LWR neutrons to proton irradiations.
3. Adjusting the cascade parameters to model proton irradiation and compare to experimental database.

The modified SOM model predictions will be compared with the data for neutron- and proton-irradiated microstructures, respectively.

4.1. Determination of parameters for LWR irradiation conditions

In modeling the microstructure evolution in LWRs, there are two classes of parameters; irradiation and material. The transition from LWR irradiation to proton irradiation will only affect the irradiation parameters. The irradiation parameters include not only the irradiation conditions, e.g., dose rate, temperature, but also parameters that may depend on the material but are influenced by irradiation conditions such as cascade efficiency (η), in-cascade interstitial clustering (f_2, f_3 and f_4), fraction of in-cascade vacancy cluster (f_{vcl}) and the radius of vacancy cluster (r_{vcl}). As described earlier, f_1, f_2 and η are fixed by MD results for neutron irradiation. The vacancy cluster size of $r_{vcl} = 0.5$ nm is fixed by calibration against fast reactor data in the original SOM model. Therefore, the fractions of in-cascade tetra-interstitial clusters, f_4, and the fraction of in-cascade vacancy clusters, f_{vcl}, are the two remaining irradiation parameters that will be fit to the existing database on LWR irradiated microstructure.

The major material parameters are migration energy of point defects and defect clusters, the pre-exponential diffusion term for point defect and defect clusters (D_2^0, D_3^0 and D_4^0). The migration energies for point defects are fixed by the original SOM model. The migration energies for interstitial clusters are fixed by the assumption discussed earlier (same as for a interstitial). The pre-exponential terms for di- and tri-interstitial clusters was determined from the value for single interstitials, as discussed earlier. Therefore, the only material parameter that will be adjusted to fit the microstructure data for LWR irradiation is the pre-exponential term for the diffusivity for tetra-interstitial clusters (D_4^0). Thus, there are three key parameters, D_4^0, f_4 and f_{vcl} that need to be fit by the database. Each are independent from the other in the model formulation, so calculations are performed by varying one parameter at a time while keeping the values of the other two fixed. In the following analysis, the individual effects of D_4^0, the pre-exponential term of diffusivity for tetra-interstitial clusters, f_4, the fraction of

interstitials surviving the cascade in the form of tetra-interstitial clusters, and f_{vcl}, the fraction of in-cascade vacancy clusters, are discussed separately.

The effect of D_4^0 on loop density and size with fixed f_4 (10%) and f_{vcl} (10%) is shown in Fig. 2(a). An increase in D_4^0 by a factor of 5 causes a decrease in loop density by ~50% without a change in dose dependence. The dose dependence in Fig. 2 matches the measurement data shown in Fig. 1. The effect of D_4^0 on the dose dependence of loop size is shown in Fig. 2(b). A factor of 5 increase in D_4^0 nearly doubled the loop size with a slight delay in the saturation. A default value of $D_4^0 = 1 \times 10^{-7}$ cm^2/s was selected for this parameter for LWR neutron irradiation.

The effect of f_4 on loop density with fixed D_4^0 (10^{-7} cm^2/s) and f_{vcl} (10%) is shown in Fig. 3(a), the results show a continuous decrease in loop density as the fraction of interstitials in tetra-interstitial clusters (f_4) decreases. The change of f_4 has little effect on the trend of dose dependence of loop density. From the f_4 changes of 10–5% and 5–2%, the amount of reduction in loop density is about the same, $\sim 2 \times 10^{17}$ cm^{-3}, corresponding to ~28% and ~40% reduction, respectively. The trends in all three cases match the data trend shown in Fig. 1. A reduction of f_4 by a factor of 5 (10–2%) caused a reduction in loop density by ~50%. It appears that a reduction in f_4 or an increase in D_4^0 by a factor of 5 results in nearly the same amount of reduction in the loop density without changing in the trend.

The effect of changes in the value of f_4 on dose dependence of loop size is shown in Fig. 3(b). Loop diameter increases as f_4 decreases because a reduction in loop nucleation allows more growth of existing loops. As f_4 decreased from 10% to 5% or from 5% to 2%, loop diameter increases by about 40% in both cases. From 10% to 2% for f_4, loop size doubled while loop density dropped by ~50%. Unlike the dose dependence of loop density, the changes of f_4 slightly alter the trend of dose dependence of loop size as f_4 decreased from 5% to 2%. It appears that the saturation of loop size was delayed when f_4 drops to 2%. Nevertheless, the trends for the three values of f_4 are still consistent with the data trend in Fig. 1. Values of $f_4 = 5\%$ and 2% matches the data trend better than $f_4 = 10\%$. The fact that a reduction of f_4 or an increase of D_4^0 by a factor of 5 has a similar effect on loop density and size suggests that a balance between the loss of small interstitial clusters to sinks by cluster diffusion and the fraction of in-cascade tetra-interstitial clustering is important for the dose dependence of loop density and size. The value of $f_4 = 2\%$ was selected as a default value for this parameter for LWR neutron irradiation.

The effect of the fraction of in-cascade vacancy clustering, f_{vcl}, on loop density as a function of dose with

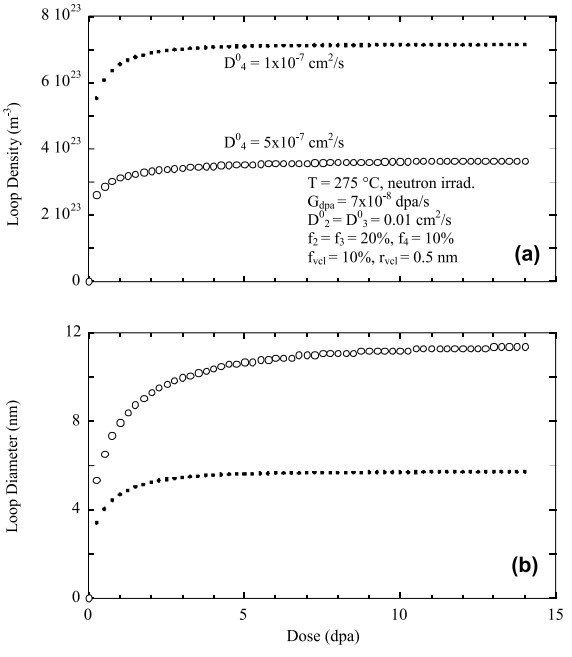

Fig. 2. Effect of pre-exponential factor D_4^0 on dose dependence of loop density (a) and size (b) for neutron irradiation at 275 °C and 7×10^{-8} dpa/s (LWR condition), calculated from the modified SOM model with $f_4 = 10\%$ and $f_{vcl} = 10\%$.

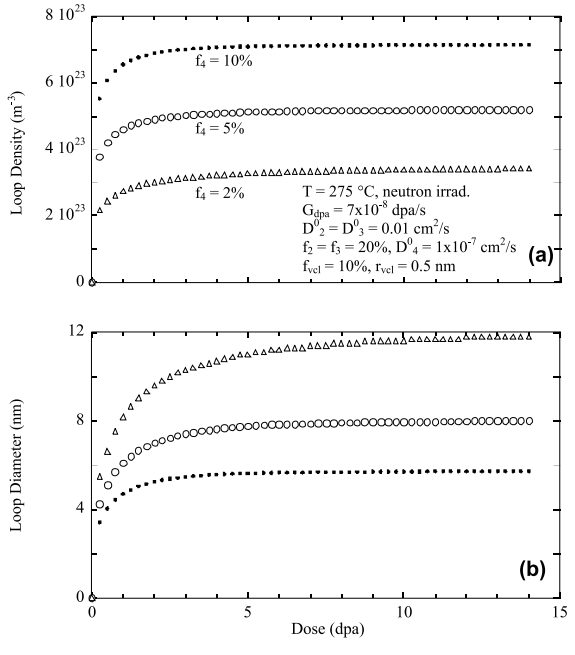

Fig. 3. Effect of in-cascade tetra-interstitial clustering f_4 on dose dependence of loop density (a) and size (b) for neutron irradiation at 275 °C and 7×10^{-8} dpa/s (LWR condition), calculated from the modified SOM model with $D_4^0 = 1 \times 10^{-7}$ cm^2/s and $f_{vcl} = 10\%$.

fixed f_4 and D_4^0 is shown in Fig. 4(a). A factor of 2 decrease in f_{vcl} increases both the magnitude and slope of the dose dependence of loop density. At $f_{vcl} = 5\%$, loop density does not saturate even at a dose of 14 dpa. This is because a lower value of f_{vcl}, means it takes longer to build up a stable overall sink strength. A stable total sink strength is probably a necessary condition for the saturation of loop density to occur. An increase in loop density at the smaller f_{vcl} is due to the reduction in sink strength for interstitials. A similar effect of f_{vcl} on loop size is shown in Fig. 4(b). Loop diameter increased and the saturation of loop size delayed with $f_{vcl} = 5\%$.

Since the data trend in Fig. 1 shows loop density saturated at 2×10^{17} cm^{-3} at dose of ~1 dpa, the value of $f_4 = 2\%$ in Fig. 3 appeared the best fit to the measurement. Thus, the parameters for the best fit of model calculation and data for LWR irradiation (275 °C and 7×10^{-8} dpa/s) are established by $f_4 = 2\%$ in Fig. 3 as follows:

- $f_4 = 2\%$ for the fraction of in-cascade tetra-interstitial clustering,
- $f_{vcl} = 10\%$ for the fraction of in-cascade vacancy clustering,
- $D_4^0 = 1 \times 10^{-7}$ cm^2/s for the diffusion of tetra-interstitial clusters.

The full list of irradiation and material parameters for LWR irradiation conditions is given in column 2 of Table 3. The model calculation with these parameters is compared with experimental measurement in Fig. 5. There is significant improvement in the model calculation in both trend and magnitude of the dose dependence of loop density and loop size. The modified model better describes the physical processes in microstructure evolution under irradiation as evidenced by the close agreement with measurements.

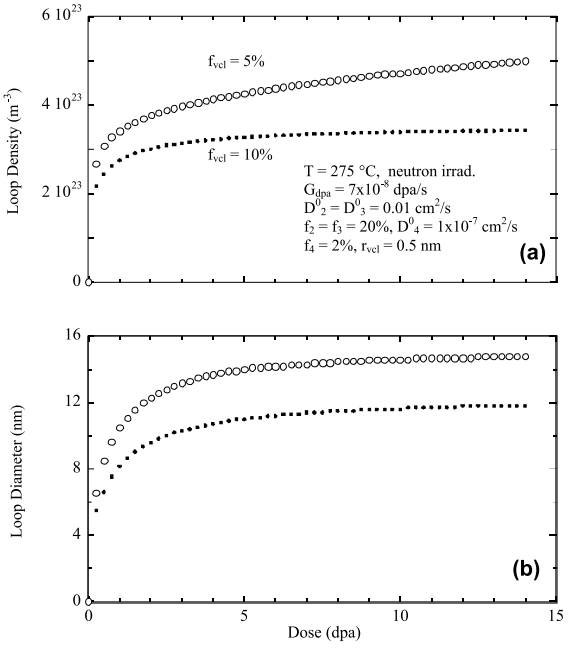

Fig. 4. Effect of in-cascade vacancy clustering f_{vcl} on dose dependence of loop density (a) and size (b) for neutron irradiation at 275 °C and 7×10^{-8} dpa/s (LWR condition), calculated from the modified SOM model with $D_4^0 = 1 \times 10^{-7}$ cm^2/s and $f_4 = 2\%$.

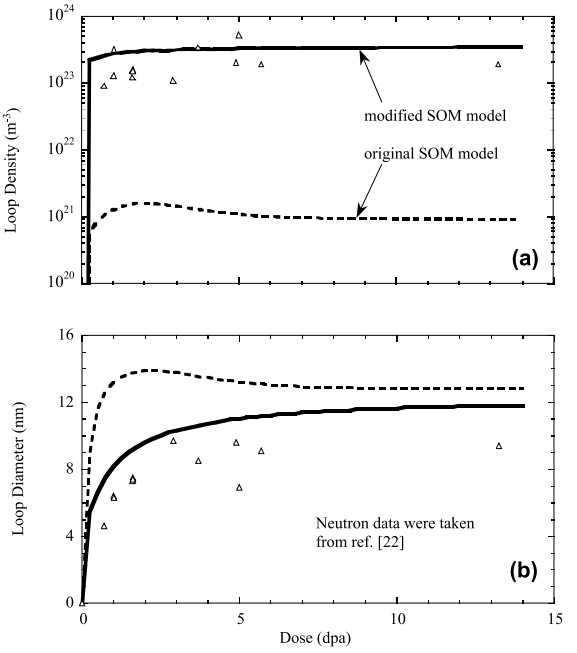

Fig. 5. Comparison of the calculated dose dependence of loop density (a) and size (b) with experimental measurements of neutron-irradiated (LWR, 275 °C) commercial purity 304 and 316 SS (data were taken from [22]).

4.2. Dose-rate dependence of loop density and size

As an approach to the higher dose rate under proton irradiation, the dose-rate responses of the calculated loop density and loop size are shown in Fig. 6(a), (b), respectively, by changing the damage rate from 7×10^{-8} dpa/s (LWR irradiation) to 7×10^{-6} dpa/s (proton irradiation). At a temperature of 275 °C, a dose-rate increase of two orders of magnitude leads to an increase in loop density by a factor of 10. This is in agreement with the experimental work by Muroga et al. [45] who found that at 400 °C, an increase of two order magnitude in dose rate results in an increase of loop density by more than one order of magnitude. An increase in the irradiation temperature from 275 to 360 °C caused a drop in the loop density, Fig. 6(a). This result suggests that in terms of temperature and dose rate change from LWR to proton irradiation, the dif-

ference in loop density will be less than one order of magnitude. The high loop density at the higher proton irradiation temperature and larger damage rate is due, at least in part, to the use of cascade parameters (f_2, f_3 and f_4) relevant to neutron irradiation, not proton irradiation.

Fig. 6(b) shows the effect of dose-rate change on the dose dependence of loop size. The lower loop size at high temperature is due to the higher loop density caused by the increase in damage rate. While the trends for 7×10^{-8} dpa/s (275 °C) and 7×10^{-6} dpa/s (360 °C) look normal, the calculation for 7×10^{-6} dpa/s (275 °C) shows an unexpected trend. The unexpected trend in dose dependence of loop size is caused by high damage rate and low irradiation temperature for neutron irradiation. The overall sink strengths build up so high that loop growth is suppressed and loops unfault at smaller sizes due to unrealistically high loop density, as determined by Eq. (11), resulting in loop size decreasing at higher doses.

It is generally assumed that, for a given dose, a higher dose rate will lead to an increase in point defect loss to bulk recombination, and less effective development of the irradiated microstructure. In fact, this statement is true only if the overall sink strength for point defects remains constant, which is not generally the case. When the microstructure development is sensitive to the dose rate, the sink strength can vary substantially. At higher dose rate, the concentration of vacancy clusters is high, which leads to a large increase in the point defect loss to vacancy clusters. A higher point defect concentration at high dose rate leads to enhanced nucleation of faulted loops by the stochastic mechanism, resulting in a high overall sink strength due to a high loop density or through loop unfaulting. Fig. 7 shows the dose-rate effect on the total sink strength for point defects. A factor of 100 increase in dose rate results in an increase in total sink strength for point defects by more than a factor of 20. As a result of the significant increase in sink strength due to the increase in the concentration of vacancy clusters and faulted loops, the fraction of interstitials lost through bulk recombination may decrease due to the increased loss of interstitials to sinks at higher dose rate.

The model is capable of tracking the defect loss to sinks and to recombination. The point defect loss to various sinks at 275 °C for dose rate 7×10^{-8} and 7×10^{-6} dpa/s in Fig. 6 is summarized in Table 2. As the dose rate increased from 7×10^{-8} to 7×10^{-6} dpa/s at 275 °C, the most significant change is the large increase in the percentage of point defects lost to vacancy clusters. A factor of 100 increase in dose rate caused: (1) the percentage of interstitials lost to recombination to drop by a factor of ~2, (2) the percentage lost to vacancy clusters to increase by a factor of ~6, and (3) the percentage lost to Frank loops and sub-grain structures to drop by factors of 2.5 and 4, respectively. The reduction of the percentage of interstitial loss to recombination at higher dose rate is due to an increase of total sink strength as shown in Fig. 7. At higher dose rate, the percentage of interstitials lost to Frank loops decreased while the loop density increased. Note that the percentage of interstitials lost to faulted loops cannot be directly

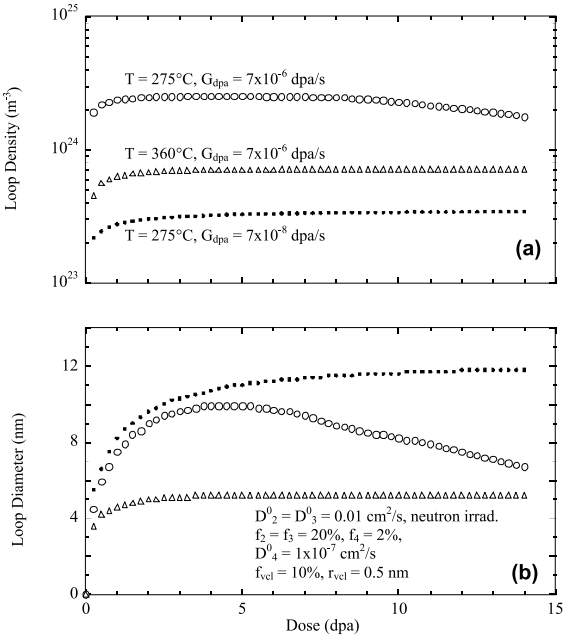

Fig. 6. Effect of dose rate (at 275 °C) and temperature (at 7×10^{-6} dpa/s) on the dose dependence of loop density (a) and size (b) for neutron irradiation, calculated from the modified SOM model.

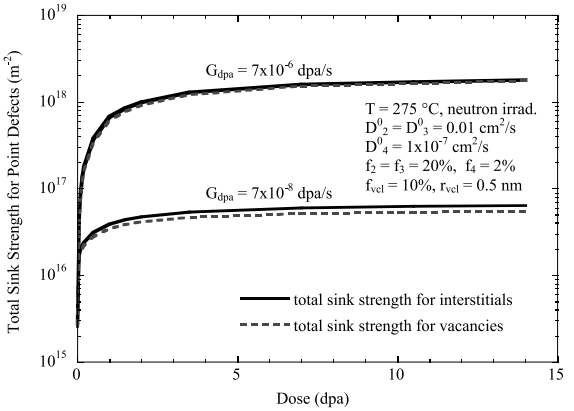

Fig. 7. Dose-rate effect on the total sink strength as a function of dose for interstitial and vacancy at 275 °C, as shown in Fig. 6, calculated from the modified SOM model.

Table 2
Point defect loss to bulk recombination and various sinks in Fig. 6, calculated using the modified SOM model

$T = 275$ °C (neutron irradiation)	% Vacancies absorbed		% Interstitials absorbed	
	7×10^{-8} dpa/s	7×10^{-6} dpa/s	7×10^{-8} dpa/s	7×10^{-6} dpa/s
Point defect loss to:				
Bulk recombination	0.12	0.06	0.12	0.06
Bubbles	1.31	0.06	1.06	0.05
Dislocations	2.07	0.11	2.08	0.10
Frank loops	64.54	25.26	64.81	25.89
Sub grain structure	25.81	6.31	20.78	5.06
Vacancy clusters	6.15	67.90	11.14	68.83
Total (%)	100.00	100.00	100.00	100.00

correlated to the faulted loop density because it also depends on the ratio of the faulted loop sink strength to the total sink strength.

The effect of dose rate on the defect concentration at 275 °C for the calculations shown in Fig. 6 is shown in Fig. 8. A rate increase from 7×10^{-8} to 7×10^{-6} dpa/s results in an increase in point defect concentration by a factor of ~8, roughly about the same amount as the increase in loop density, Fig. 6. The concentration of tetra-interstitial clusters is about 4 orders of magnitude higher than that of single-, di- and tri-interstitials at both dose rates. This is mainly because of the extremely small pre-exponential term of the diffusivity for the tetra-interstitial cluster diffusion.

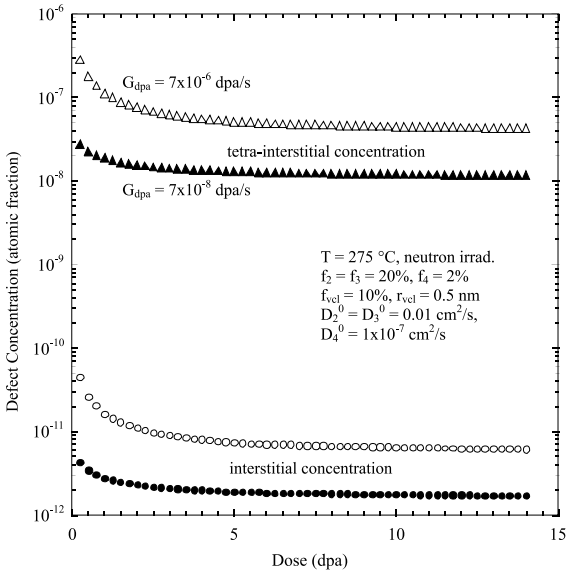

Fig. 8. Dose-rate effect on the defect concentrations as a function of dose between dose rate of 7×10^{-8} dpa/s (solid symbol) and 7×10^{-6} dpa/s (open symbol) in Fig. 6, calculated from the modified SOM model.

4.3. Temperature dependence of loop density and size

The temperature response of loop density and size as a function of dose for neutron irradiation is shown in Fig. 9(a), (b). At a damage rate of 7×10^{-8} dpa/s, loop density decreases monotonically with temperature as expected. From 275 to 360 °C, loop density is reduced by more than a factor of 2. This trend is in reasonable agreement with measurements [46], but the magnitude of the reduction in loop density is less than in the measurements.

The effect of irradiation temperature on loop size is shown in Fig. 9(b). Again, the trend is in agreement with measurement. Loop diameters increase with tempera-

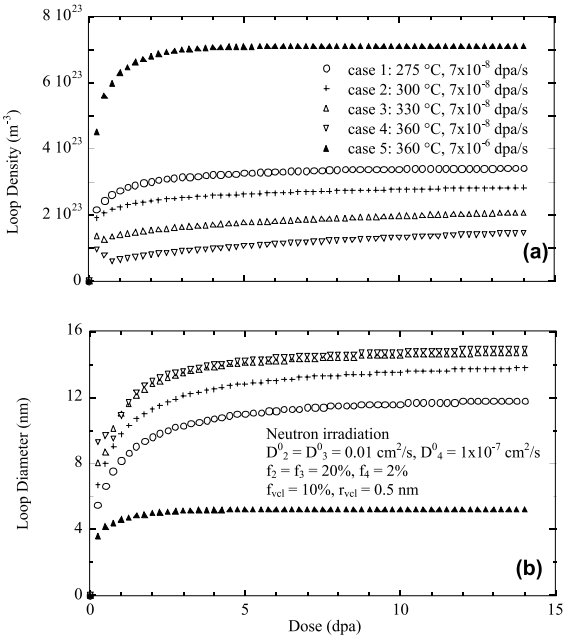

Fig. 9. Effect of temperature on the dose dependence of loop density (a) and size (b) for neutron irradiation at 7×10^{-8} dpa/s, calculated from the modified SOM model.

ture for a given damage rate as expected. In all the cases, loop size increases rapidly at low dose. At high dose rate, the saturation occurs earlier than in the lower dose-rate cases. The effect of combining a higher dose rate and higher temperature (relevant to proton irradiation conditions) is also shown. Compared to the LWR case, the result is an increase in loop density by a factor of 5 and a drop in loop size.

4.4. Effect of cascade efficiency and helium generation on loop density and size at 360 °C

The effect of cascade efficiency and helium production on the dose dependence of loop density and size relevant to proton irradiation conditions is shown in Fig. 10(a), (b). The elimination of He production has no effect on loop size or density as evidenced by the overlap of 1 and 2. An increase in the cascade efficiency from 0.33 to 0.90 causes a small increase in loop density and a reduction in loop size by about 25%. The unrealistically smaller loop sizes at saturation in all three cases is due to the high loop density caused by high dose rate. The following section treats the transition from neutron irradiation to proton irradiation, and deals principally with the fraction of in-cascade interstitial clustering.

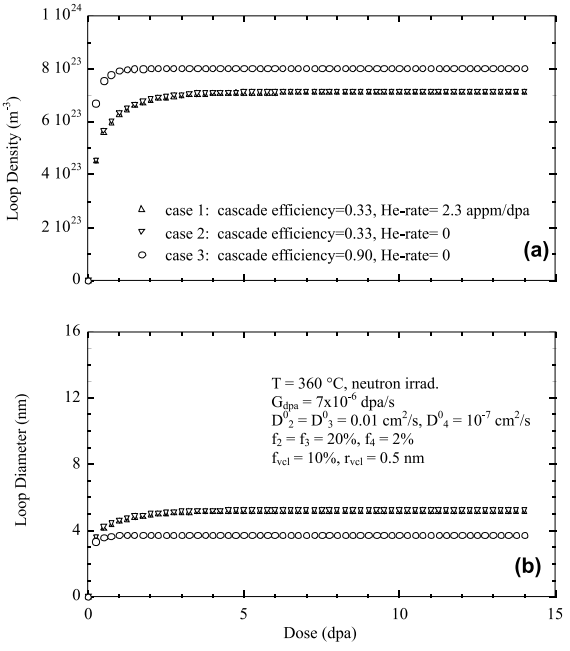

Fig. 10. Effect of helium production and cascade efficiency on dose dependence of loop density (a) and size (b), calculated from the modified SOM model for neutron irradiation at 360 °C.

4.5. Parameter determination for proton irradiation relevant to LWR irradiation conditions

For the case of proton irradiation, all material parameters remain the same as for neutron irradiation and only the irradiation parameters are allowed to change. Guided by MD results in [40], a value of 0.9 was chosen for the cascade efficiency due to the reduced cascade energy for proton irradiation. Of the remaining irradiation parameters given in Table 3, only those parameters which are associated with clustering are affected by the change in irradiating particle and condition. Fig. 11 shows a series of plots of loop density and loop size in which the values of f_2, f_3, f_4 and f_{vcl} were varied over a narrow range. The measurements of loop density and loop size were also included in the plot.

As discussed above, the MD results from [40] were used to define the range of values for the fractions of in-cascade interstitial clustering for 3.2 MeV proton irradiation to be $f_1 = f_2 = 1$–2% and $f_4 = 0.1$–0.2%. The range of the value of f_{vcl} was chosen to be similar to that for neutron irradiation, as this was required for the model to produce reasonable results. This is a weak point in the modeling of proton irradiation. The inconsistent treatment of in-cascade interstitial and vacancy clustering when changing from neutron to proton irradiation is in part due to the over-simplified treatment for vacancy clusters. That is, vacancy clusters are assumed to be produced only from cascades and are only of one single size.

In Fig. 11 shows the effect of several irradiation parameters; f_2, f_3 and f_{vcl} on loop density and size. Note that despite an increase in the fraction of di- and

Table 3
The parameters for the better fit of model calculation and data for proton irradiation (360 °C and 7×10^{-6} dpa/s) established from case 2 in Fig. 11, with the key parameters for neutron irradiation (275 °C and 7×10^{-8} dpa/s)

Parameter	LWR neutron irradiation	Proton irradiation	Comments
η	0.33	0.90	Fixed by MD results
$f_2 = f_3$	20% each	1%	Fixed by MD results
f_4	2%	0.1%	Fit to data
f_{vcl}	10%	10%	Fit to data
r_{vcl}	0.5 nm	0.5 nm	Fixed by calibration for fast reactor
$D^0_2 = D^0_3$	10^{-2} cm^2/s	10^{-2} cm^2/s	Fixed by assumption
D^0_4	10^{-7} cm^2/s	10^{-7} cm^2/s	Fit to data

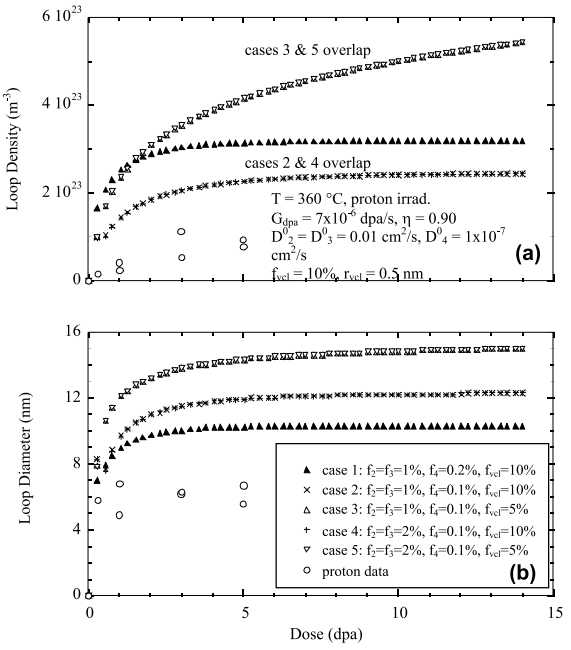

Fig. 11. Dose dependence of loop density (a) and size (b) under various conditions for proton irradiation at 360 °C and 7×10^{-6} dpa/s, calculated from the modified SOM model.

tri-interstitial clustering (f_2, f_3) by a factor of 2 the loop density and diameter overlap for cases 2 and 4. This is due to relatively high mobility for di- and tri-interstitial clusters compared to that for tetra-interstitial clusters, as well as the fact that the model assumed that thermal dissociation could occur for di- and tri-interstitial clusters, but not for tetra-interstitial clusters. The overlap between cases 3 and 5 is caused by the same reason as for cases 2 and 4. From case 2 to 3, a decrease in the fraction of in-cascade vacancy clustering (f_{vcl}) by a factor of 2 results in a significant change in both loop density and the trend. The loop densities do not saturate in case 3 even at dose up to 14 dpa and the densities are too high compared to measurement data. The model calculations are compared with the proton data in Fig. 11. It appears that cases 2 and 4 are consistent with measured data trend. For the dose dependence of loop size in Fig. 11(b), it appears that cases 1 and 2 are a better fit to the measured data. Considering both loop density and size, case 2 will be used for proton irradiation.

The thermal stability plus the extremely low mobility for tetra-interstitial clusters means that the fraction of in-cascade tetra-interstitials, f_4, has a stronger effect on loop density than does the fraction of di- and tri-interstitial clusters. The large difference between the impacts of tetra-interstitial clusters and di- or tri-interstitial clusters on the loop density is caused by the assumption made in the description of cluster mobility. A 5 order of magnitude difference between D^0_4 and D^0_3 or D^0_2 may not be physically realistic. Unless a reliable result from MD simulation can be used for the description of cluster mobility (if it can be justified by some experimental data), the treatment of cluster mobility in the current model is very limited. This is due to the assumptions that: (1) an interstitial cluster has the same migration energy as a single interstitial, (2) the diffusivity of tetra-interstitial clusters is significantly lower than di- and tri-interstitials, and (3) the sink strengths are the same for interstitial clusters as for a single interstitial. It appears more reasonable to assume that the contribution of di- or tri-interstitial clusters to the microstructure development should be comparable to tetra-interstitial clusters.

The key parameters for the modeling of the proton-irradiated microstructure are thus the following:

- $f_4 = 0.1\%$ for the fraction of in-cascade tetra-interstitial clustering,
- $\eta = 0.90$ for cascade efficiency for proton irradiation,
- $f_{vcl} = 10\%$ for the fraction of in-cascade vacancy clustering.

These parameters are listed in Table 3, together with that for neutron irradiation. Compared to neutron irradiation in LWRs, under proton irradiation, in-cascade interstitial clustering is reduced by a factor of 20 while the distribution of in-cascade interstitial clusters is the same as for neutron irradiation. The same numbers for the fraction of vacancy clustering ($f_{vcl} = 10\%$) and size ($r_{vcl} = 0.5$ nm) are used for both neutron and proton irradiation. This is necessary to preserve the calculated loop density and trend in agreement with the measurements. The use of the same parameters for vacancy clusters between neutron and proton irradiation may reflect the problems in the oversimplified treatment of vacancy clusters (single size, immobile). The model calculation with these parameters is compared with measurement and is shown in Fig. 12(a), (b) for loop density and size, respectively. The model calculations for both dose dependence and magnitude of the loop density and size are consistent with the proton-irradiated microstructure. The model prediction is higher than the measurement data.

The calculation of the source terms in Eqs. (3)–(5) can be carried out for both in-cascade and classical nucleation of di-, tri- and tetra-interstitials in order to examine the differences between neutron (275 °C, 7×10^{-8} dpa/s) and proton irradiation (360 °C, 7×10^{-6} dpa/s). The results indicate that nucleation rate for tetra-interstitials (treated as loops) due to in-cascade interstitial clustering increased from neutron irradiation (1.17×10^{-10} # tetra-int./atom/s) to proton irradiation (3.15×10^{-9} # tetra-int./atom/s), despite the reduction of f_2, f_3 and f_4 in proton irradiation. The corresponding classical nucleation rate for tetra-interstitials increased by a factor of ~1000 from neutron irradiation (~10^{-16} # tetra-int./atom/s) to proton

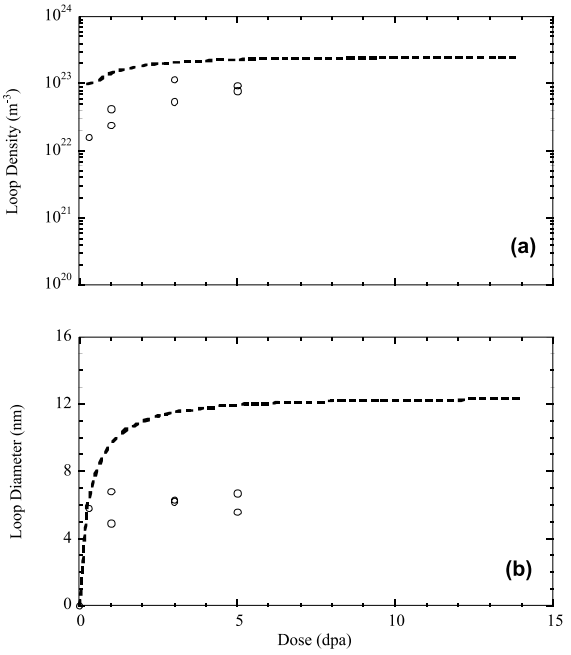

Fig. 12. Comparison of the calculated dose dependence of loop density (a) and size (b) with experimental measurements of proton-irradiated (3.2 MeV, 360 °C) commercial purity 304 and 316 SS.

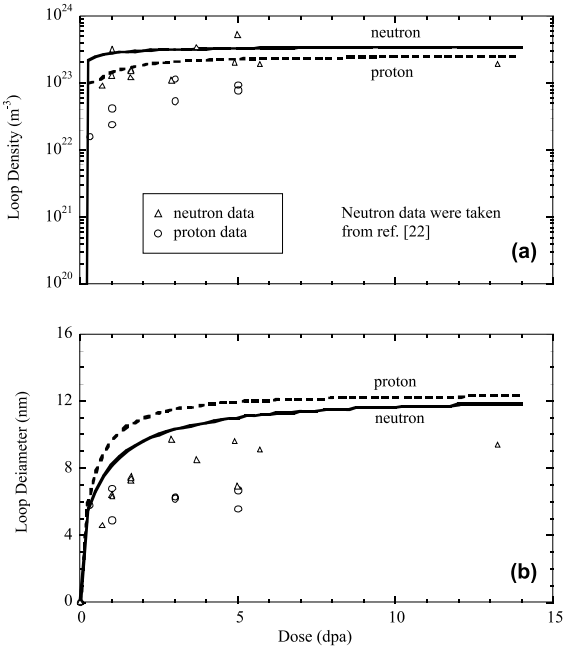

Fig. 13. Comparison of the calculated dose dependence of loop density (a) and size (b) with experimental measurements of neutron-irradiated (△, LWR, 275 °C) (data were taken from [22].) and proton-irradiated (○, 3.2 MeV, 360 °C) commercial purity 304 and 316 SS.

irradiation ($\sim 10^{-13}$ # tetra-int./atom/s). Thus, the total nucleation rate at a given dose for tetra-interstitials for proton irradiation at 360 °C and 7×10^{-6} dpa/s is higher than that for neutron irradiation at 275 °C and 7×10^{-8} dpa/s by a factor of ~30. Note that the nucleation rate for di-, tri- and tetra-interstitials cannot be directly related to the measured loop density. It is the interstitial cluster nucleation rate and loss rate of di-, tri- and tetra-interstitials, the unfaulting of Frank loops, and the irradiation dose that determine the measured loop density. Note that for proton irradiation with reduced f_2, f_3 and f_4 (by a factor of 20) compared to that for LWR neutron irradiation, loop nucleation is still driven by in-cascade interstitial clustering due to higher dose rate and cascade efficiency and lower sink strength at higher temperature.

4.6. Comparison of model calculation with measurements

The results of calculations using the modified SOM model for both neutron and proton irradiation, along with the measured data from neutron- and proton-irradiated samples are plotted together in Fig. 13(a), (b) for loop density and size, respectively. In Fig. 13, the solid lines are the calculated loop density and size for LWR neutron irradiation at 275 °C and 7×10^{-8} dpa/s, and the dashed lines are for proton irradiation at 360 °C and 7×10^{-6} dpa/s. The triangle symbols are measurements for neutron irradiation at 275 °C and 7×10^{-8} dpa/s [22]. The circle symbols are measurements for proton irradiation at 360 °C and 7×10^{-6} dpa/s. The agreement between the model calculations and measurement is excellent. The difference between model calculation and the measured data is less than a factor of 2 for both neutron and proton cases, instead of a factor of 100 difference in the original SOM model calculation. It is encouraging that the modified SOM model predicts less than a factor of 2 in difference in faulted loop density between neutron and proton irradiation at the specified irradiation conditions, consistent with the microstructure measurements [38]. This provides support for the use of proton irradiation as a tool for emulating the irradiated microstructural that results from irradiation in LWRs.

A major concern in conducting proton irradiation to study the neutron-irradiated microstructure is on the difference in the size and production of displacement cascades. Neutrons produce much larger cascades. Loop nucleation is driven by the in-cascade interstitial clustering rather than classic nucleation of dislocation loops at LWR temperature and dose rate. Proton irradiation produces smaller and spatially separated cascades. Although the fraction of interstitials forming in-cascade interstitial clusters is less than for neutrons

(f_2, f_3 and f_4 reduced by a factor of 20), more interstitials survive cascade recombination due to the higher cascade efficiency for proton irradiation ($0.33 \rightarrow 0.90$). This leads to only a factor of $\sim$7.3 reduction in the total amount interstitials in the in-cascade interstitial clustering for proton irradiation. The higher dose rate and the lower sink strength at higher temperature in proton irradiation result in equivalent microstructure development as for neutron irradiation. The model suggests that, for both neutron irradiation (LWR core condition) and proton irradiation (relevant to LWR core), the nucleation of Frank loops are driven by in-cascade interstitial clustering. Classical nucleation of Frank loops is insignificant under irradiations relevant to LWR cores.

5. Conclusions

The modeling of microstructure evolution under irradiation conditions relevant to LWR is achieved. The microstructure model developed by Stoller and Odette for fast reactor can be modified to apply to LWR irradiation conditions. The major modifications are the inclusion of in-cascade interstitial clustering and the loss of small interstitial clusters to sinks by cluster diffusion. The irradiation-based parameters fit to the existing LWR dislocation microstructure database were: the fraction of interstitials surviving the cascade in the form of tetra-interstitial clusters, $f_4 = 2\%$, the pre-exponential term for the diffusivity of tetra-interstitial clusters $D_4^0 = 1 \times 10^{-7}$ cm^2/s, and the fraction of in-cascade vacancy clusters, $f_{\mathrm{vcl}} = 10\%$. The fit produces good agreement in the dose dependence of dislocation loop density and size evolution.

Proton irradiation produced an equivalent irradiated microstructure as that from irradiation in an LWR core. The calculated dose dependence of loop density and loop size are in agreement with the measurements. The model predicts less than a factor of 2 difference in loop density between neutron and proton irradiation in excellent agreement with the factor of $\sim$1.5 identified experimentally from the comparison of neutron- and proton-irradiated microstructure measurements [47]. The modified model provides the correct response to the measured changes in irradiation temperature and damage rate.

In proton irradiation, the fraction of interstitials in clusters is reduced by a factor of 20 compared to neutron irradiation. But the higher dose rate and cascade efficiency and the lower sink strength at the higher temperature in proton irradiation results in a higher nucleation rate of tetra-interstitials. In both cases, Frank loop nucleation is driven by in-cascade interstitial clustering and classical nucleation of loops is insignificant. These somewhat compensating effects explain the equivalence of the dislocation loop density and size between neutron and proton irradiation.

Acknowledgements

The authors would like to thank Dr Danny Edwards and Dr Stephen Bruemmer at the Pacific Northwest National Laboratory for their support and contribution to this work. Many thanks to Dr Ed Simonen for helpful discussion and suggestion. This work was supported by the Electric Power Research Institute under contract number WO4068-26, US Department of Energy under grant DE-FG02-93ER-12310 at the University of Michigan and the Material Science Branch of the Office of Basic Energy Science, US Department of Energy, under contract DE-ACO6-76RL0 1830 with Battelle Memorial Institute at Pacific Northwest National Laboratory. Research at the Oak Ridge National Laboratory was sponsored by the Division of Materials Sciences and Engineering and the Office of Fusion Energy Sciences, US Department of Energy under contract DE-AC05-00OR22725 with UT-Battelle, LLC.

References

[1] A.D. Brailsford, R. Bullough, J. Nucl. Mater. 44 (1972) 121.
[2] A.D. Brailsford, R. Bullough, M.R. Hayns, J. Nucl. Mater. 60 (1976) 246.
[3] R. Bullough, M.R. Hayns, in: SM Archives, vol. 3, Noordhoof International, The Netherlands, 1978, p. 73.
[4] J.L. Katz, H. Wiedersich, J. Chem. Phys. 55 (1971) 1414.
[5] M. Kiritani, J. Phys. Soc. Jpn. 35 (1973) 95.
[6] M.R. Hayns, J. Nucl. Mater. 56 (1975) 267.
[7] G.R. Odette, S.C. Langley, in: Radiation Effects and Tritium Technology for Fusion Reactors, CONF-750989, vol. I, 1975, p. 395.
[8] K.C. Russell, in: Consultants Symposium, AERE-R7934, AERE Harwell, 1975, p. 158.
[9] L.K. Mansur, Nucl. Tech. 40 (1978) 5.
[10] W.G. Wolfer, L.K. Mansur, J.A. Sprague, in: Proceedings of International Conference, AIME, New York, 1977, p. 841.
[11] N.M. Ghoniem, D.D. Cho, in: The Influence of Vacancy Clustering on the Early Stages of Interstitial Loop Formation and Growth, UCLA-ENG-7845, University of California, Los Angeles, 1978.
[12] R.M. Mayer, L.M. Brown, U. Gosele, J. Nucl. Mater. 95 (1980) 44.
[13] R.E. Stoller, G.R. Odette, J. Nucl. Mater. 103&104 (1981) 1361.
[14] G.R. Odette, R.E. Stoller, J. Nucl. Mater. 122&123 (1984) 514.
[15] L.K. Mansur, W.A. Coghlan, J. Nucl. Mater. 119 (1983) 1.
[16] R.E. Stoller, G.R. Odette, in: F.A. Garner, N.H. Packan, A.S. Kumar (Eds.), Radiation Induced Changes in Microstructure: 13th International Symposium (part I), ASTM STP 955, ASTM, Philadelphia, PA, 1987, p. 371.

[17] R.E. Stoller, in: Microstructural Evolution in Fast-Neutron-Irradiated Austenitic Stainless Steels, ORNL-6430, Oak Ridge National Laboratory, December, 1987.
[18] G.S. Was, T.R. Allen, J.T. Busby, J. Gan, D. Damcott, D. Carter, M. Atzmon, E.A. Kenik, Mater. Res. Soc. Symp. Proc. 540 (1999) 421.
[19] J. Gan, T. Allen, G.S. Was, Mater. Res. Soc. Symp. Proc. 439 (1997) 445.
[20] J.T. Busby, T.R. Allen, J. Gan, G.S. Was, in: 18th International Symposium on Environmental Degradation of Materials in Nuclear Power Systems – Water Reactors, Amelia Island, FL, 1997, p. 758.
[21] P.J. Maziasz, ORNL-6121, Oak Ridge National Laboratory, 1985.
[22] S.M. Bruemmer, EPRI report 4068-20, October, 1997.
[23] R.E. Stoller, J. Nucl. Mater. 276 (2000) 22.
[24] R.E. Stoller, G.R. Odette, B.D. Wirth, J. Nucl. Mater. 251 (1997) 49.
[25] N. Yoshida, H. Murakami, T. Muroga, in: Proceedings International Symposium on Behavior of Lattice Imperfections in Materials, Osaka, 1985, p. 18.
[26] K. Murakami, master thesis, Kyushu University, 1986.
[27] H. Watanabe, A. Aoki, H. Murakami, T. Muroga, N. Yoshida, J. Nucl. Mater. 155–157 (1988) 815.
[28] N. Yoshida, J. Nucl. Mater. 174 (1990) 220.
[29] S. Kojima, T. Yoshiie, K. Hamada, K. Satori, M. Kiritani, J. Nucl. Mater. 191–194 (1992) 1155.
[30] Y.N. Osetsky, A. Serra, V. Priego, F. Gao, D.J. Bacon, Mater. Res. Soc. Symp. Proc. 527 (1998) 49.
[31] Y.N. Osetsky, A. Serra, V. Priego, Mater. Res. Soc. Symp. Proc. 527 (1998) 59.
[32] V.A. Borodin, A.I. Ryazanov, J. Nucl. Mater. 256 (1998) 47.
[33] R.E. Stoller, in: R.K. Nanstad et al. (Eds.), Effects of Radiation on Materials: 18th International Symposium, ASTM 1325, 1997.
[34] P. Zhao, Y. Shimomura, Jpn. J. Appl. Phys. 36 (1997) 7291.
[35] Y.N. Osetsky, D.J. Bacon, A. Serra, B.N. Singh, S.I. Golubov, J. Nucl. Mater. 276 (2000) 65.
[36] H.L. Heinisch, B.N. Singh, S.I. Golubov, J. Nucl. Mater. 276 (2000) 59.
[37] R.A. Johnson, J. Nucl. Mater. 83 (1979) 147.
[38] J. Gan, PhD dissertation, The University of Michigan, 1999.
[39] A. Jenssen, L.G. Ljungberg, in: 7th International Symposium on Environmental Degradation of Materials in Nuclear Power System – Water Reactors, Breckenridge, CO, 1995, p. 1043.
[40] R.E. Stoller, L.R. Greenword, J. Nucl. Mater. 271&272 (1999) 57.
[41] J.T. Stanley, J.R. Cost, J. Phys. F (1984) 1801.
[42] O. Dimitrov, C. Dimitrov, J. Nucl. Mater. 105 (1982) 39.
[43] F.W. Young, J. Nucl. Mater. 69&70 (1978) 310.
[44] G.S. Was, Irradiation Effects In metals And Alloys, University of Michigan, 1992.
[45] T. Muroga, Y. Miyamoto, H. Watanabe, N. Yoshida, J. Nucl. Mater. 155–157 (1988) 810.
[46] S.J. Zinkle, P.J. Maziasz, R.E. Stoller, J. Nucl. Mater. 206 (1993) 270.
[47] J. Gan, G.S. Was, J. Nucl. Mater. 297 (2001) 161 (erratum 298 (2001) 341).